nature astronomy

Supplementary information

https://doi.org/10.1038/s41550-026-02820-x

Different architecture of Jupiter and Saturn satellite systems from magnetospheric cavity formation

In the format provided by the authors and unedited

Table of contents

Time evolutions of the magnetic field strength at planetary surfaces

Supplementary Figure 1 shows the magnetic field strength at the surface of the two gas giants over 5 Gyr. The critical pressure at which hydrogen metallization occurs sets the upper and lower limits of the magnetic field strength [1], that is, 1 Mbar and 2 Mbar, respectively. Most of the envelope of young Jupiter is occupied by metallic hydrogen, whereas the metallic hydrogen layer in young Saturn appears only near the core surface (see Supplementary Figure 2). We find that young Jupiter has a surface magnetic field as strong as 100 G, whereas young Saturn has a relatively weak surface magnetic field of $\sim$ 1 G. Larger convective heat flux in the dynamo region yields a stronger magnetic field in a planet. As a gas giant radiates heat into space, the magnetic field strength decreases monotonically with time. Since gravitational contraction expands the region of metallic hydrogen in young Saturn, the magnetic field strength gradually increases until $\sim$ 100 Myr. And then, the magnetic field strength of young Saturn continues to decrease monotonically due to radiative cooling, the same as for young Jupiter. Despite an extensive dynamo region in mature

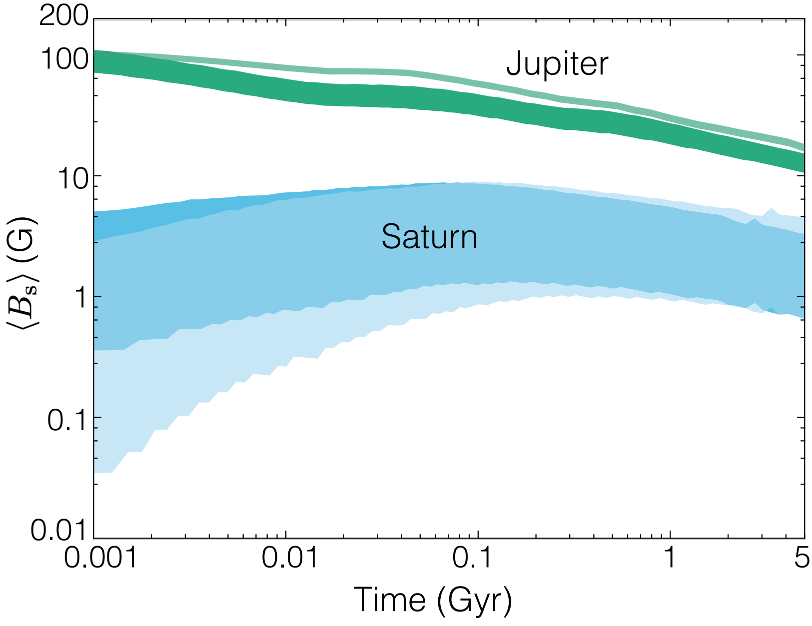

Supplementary Figure 1 Dipole magnetic field strength at the equator on the surface of Jupiter and Saturn. Light and dark colors represent the Jupiter model with no core and $20M_\oplus$ and the Saturn model with a core of 10 $M_\oplus$ and 20 $M_\oplus$, respectively. The upper and lower limits correspond to the metallization of hydrogen at 1 Mbar and 2 Mbar. Note that there is no significant difference in $\langle B_s \rangle$ between the two Jupiter models, whereas young Saturn with the core of $10M_\oplus$ has a weaker $\langle B_s \rangle$ for $\lesssim$ 0.1 Gyr. Note that the ranges of dipole magnetic field strength in the two Saturn models overlap around 1 G.

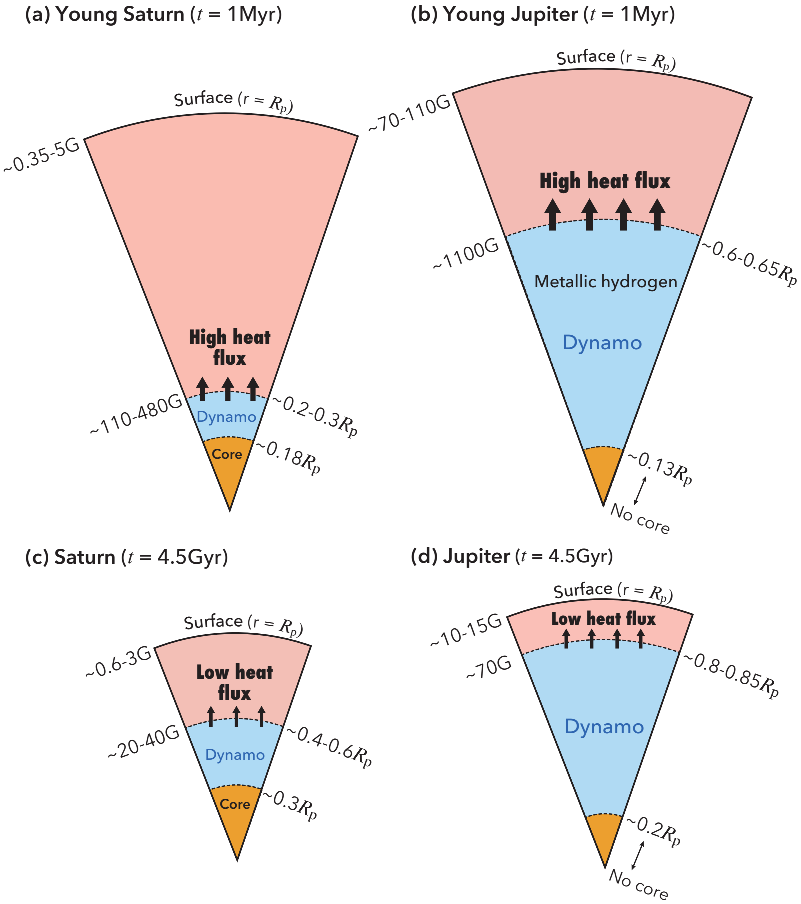

Supplementary Figure 2 Schematic pictures of the interiors of Jupiter and Saturn at 1Myr and 4.5Gyr. In the interior models of Jupiter and Saturn, the core masses range from 0 to $20M_\oplus$ and 10 to $20M_\oplus$, respectively. Hydrogen metallization is assumed to occur at $P = 1 - 2\,\mathrm{Mbar}$. The orange, blue, and red regions mean the core, the dynamo region, and the envelope in which metallization of hydrogen does not occur, respectively. The numbers on the left and right represent the magnetic field strengths and the locations of the surface of each layer.

Jupiter and Saturn, their surface magnetic fields are as weak as $1 - 10\,\mathrm{G}$ due to low convective heat fluxes.

Tidal evolution of forming satellites

The tidal deformation of a planet changes the orbits of its satellites. Tidal torque acting on a satellite is written as

$$\frac{\dot{a}}{a} = \mathrm{sign}(\omega_\mathrm{p} - \Omega_\mathrm{s}) \frac{3k_2}{Q_\mathrm{p}} \left(\frac{R_\mathrm{p}}{a}\right)^5 \left(\frac{M_\mathrm{moon}}{M_\mathrm{p}}\right) \Omega_\mathrm{s}, \tag{1}$$

where a is the semimajor axis of satellites, $M_{\rm moon}$ and $M_{\rm p}$ are the mass of a satellite and a planet, $\omega_{\rm p}$ is the rotation angular velocity of a planet, $\Omega_{\rm s}$ is the Keplerian frequency of a satellite, k_2 is the Love number, and $Q_{\rm p}$ is the tidal dissipation factor of a planet [2]. The timescale for changes to the orbit of a satellite due to tidal torque is given by

$$t_a \sim 4.7 \left(\frac{k_2}{0.3}\right)^{-1} \left(\frac{Q_{\rm p}}{3\times 10^4}\right) \left(\frac{R_{\rm p}}{R_{\rm J}}\right)^{-5} \left(\frac{a}{4\,R_{\rm J}}\right)^{13/2} \left(\frac{M_{\rm p}}{M_{\rm J}}\right)^{1/2} \left(\frac{M_{\rm moon}}{0.01\,M_\oplus}\right)^{-1} \text{Gyr}, \tag{2}$$

where $t_a = \left|a/\dot{a}\right|$ and $R_{\rm J}$ is the Jupiter's radius. The $Q_{\rm p}$-value of Jupiter [3] (Saturn [4]) is estimated to lie between 10^4 (10^2) and 10^5 (10^5). According to equation (2), the orbital change of a satellite occurs slowly over Gyr.

A satellite beyond the corotation radius, which is defined as $a_{\rm cr} = \left(GM_{\rm p}/\omega_{\rm p}^2\right)^{1/3}$, moves outward due to tidal interaction. Assuming a gas giant with a constant moment of inertia, that is, $\omega_{\rm p}(t) = \omega_0 \left(R_{\rm p}/R_{\rm J}\right)^{-2}$, the time-dependent corotation radius can be described as $a_{\rm cr} = a_{\rm cr}^0 \left(R_{\rm p}/R_{\rm J}\right)^{4/3}$, where ω_0 is the rotation angular velocity of the present-day Jupiter ($P_{\rm rot} = 9.925$ hrs) or Saturn ($P_{\rm rot} = 10.625$ hrs) and $a_{\rm cr}^0$ is the corotation radius of the present-day Jupiter or Saturn. We do not consider the angular momentum exchange between Jupiter (Saturn) and the formed satellites through tidal interactions

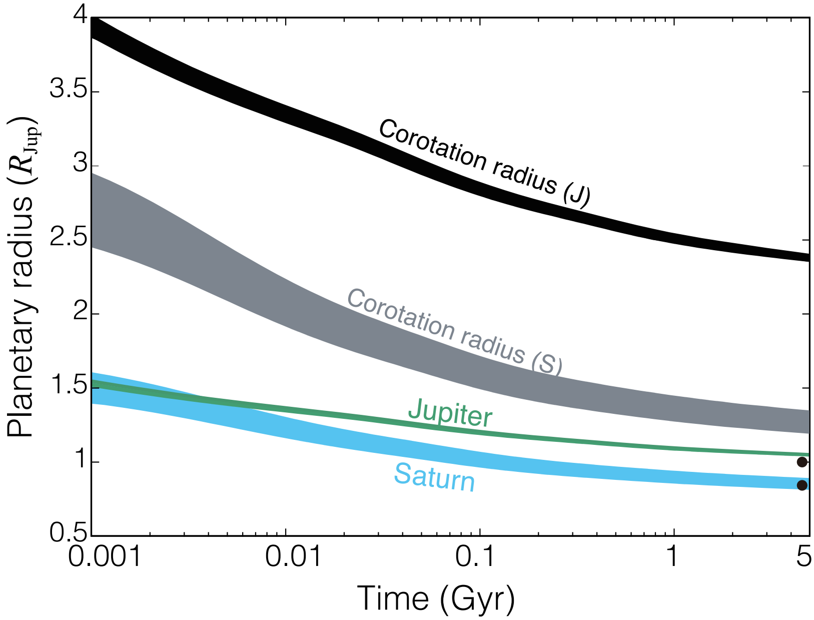

Supplementary Figure 3 Radius evolution of a Jupiter-mass (green) and Saturn-mass planet (cyan) over 5 Gyrs. Black filled circles are the radii of the present-day Jupiter and Saturn. The corotation radii of a Jupiter-mass and a Saturn-mass planet are shown in black and gray. The shaded regions represent interior models of Jupiter with an inner core of $\leq 20 M_\oplus$ and Saturn with a $10 - 20 M_\oplus$ core as in Supplementary Figure 1.

and magnetic interactions. We simulate the thermal evolution of Jupiter and Saturn for 5Gyr. Supplementary Figure 3 shows that the radius of a Jupiter-mass planet with an inner core of $\leq 20M_\oplus$ and a Saturn-mass planet with a $10-20M_\oplus$ core shrinks from $\sim 1.5\,R_\mathrm{J}$ to $\sim 1\,R_\mathrm{J}$ over ~ 1 Gyr. The corotation radius of a young Jupiter-mass planet aged $1-10$ Myr was beyond $3\,R_\mathrm{J}$. Thus, the location of satellite formation around young Jupiter is expected to be exterior to its corotation radius. The orbits of the satellites that formed in our N-body simulations gradually expand over Gyr.

Other disk models

The orbital configuration of Galilean-like moons in our N-body simulations favors $\alpha = 10^{-4}$ and enhanced dust opacities, specifically, the amount of silicate and icy dust grains are doubled from the original value [5]. Supplementary Figure 4 shows the circum-Jovian disk models with different values of the viscous parameter α and enhanced and non-enhanced dust opacities. In any case, a magnetospheric cavity can form around young Jupiter with $\langle B_\mathrm{s}\rangle = 100$ G. Note that our disk models are insensitive to $\langle B_\mathrm{s}\rangle$ because whether and where a magnetospheric cavity forms is determined by the extent to which the sufficiently ionized gas is coupled with the planetary magnetic field.

The magnetospheric accretion may occur temporarily if the magnetic field of young Saturn becomes as strong as 3 G (Supplementary Figure 5). However, young Saturn has $\langle B_\mathrm{s}\rangle \lesssim 3$ G before disk dissipation (see Supplementary Figure 1). Also, a higher $\langle B_\mathrm{s}\rangle$ for young Saturn is not compatible with the observed value of present-day Saturn.

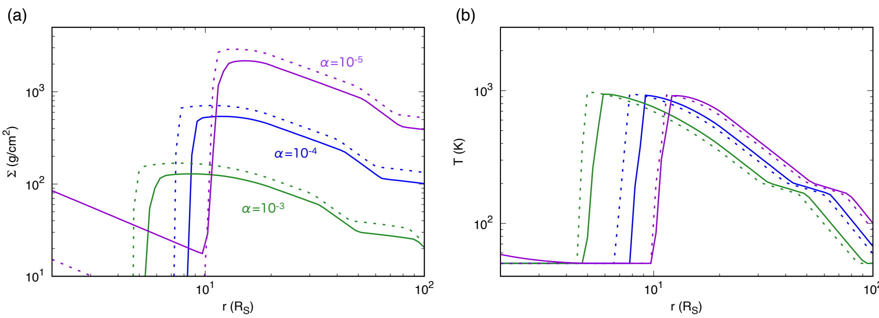

Supplementary Figure 4 Models for circum-Jovian disks with different parameters. Surface density (a) and temperature (b) distributions for $\alpha = 10^{-3}$, 10^{-4}, 10^{-5}. The fiducial model in the main text corresponds to the solid blue curves. The solid and dashed lines are CPD models with two-fold dust opacities and non-enhanced ones, respectively.

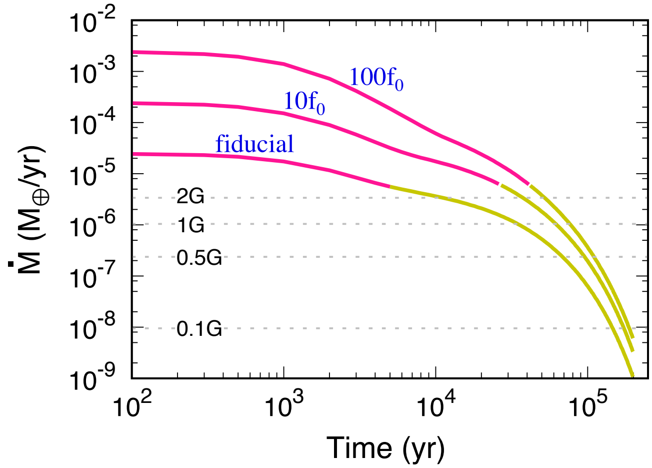

Supplementary Figure 5 Mass accretion rate onto young Saturn from the circum-Saturnian disk at the last stage of disk evolution, i.e., the dissipating phase. The pink and yellow curves indicate $R_m > 1$ and $R_m < 1$, respectively. The different lines indicate the different steady states with fiducial, and 10- and 100-times larger mass infall rate f_0, respectively.

Supplement to *N*-body simulation

In the main text, Figure 4 shows the results of N-body simulations for both Jupiter and Saturn. Here we look at these results in more detail, and also at the probability of the results shown in Figure 4 based on additional N-body simulations.

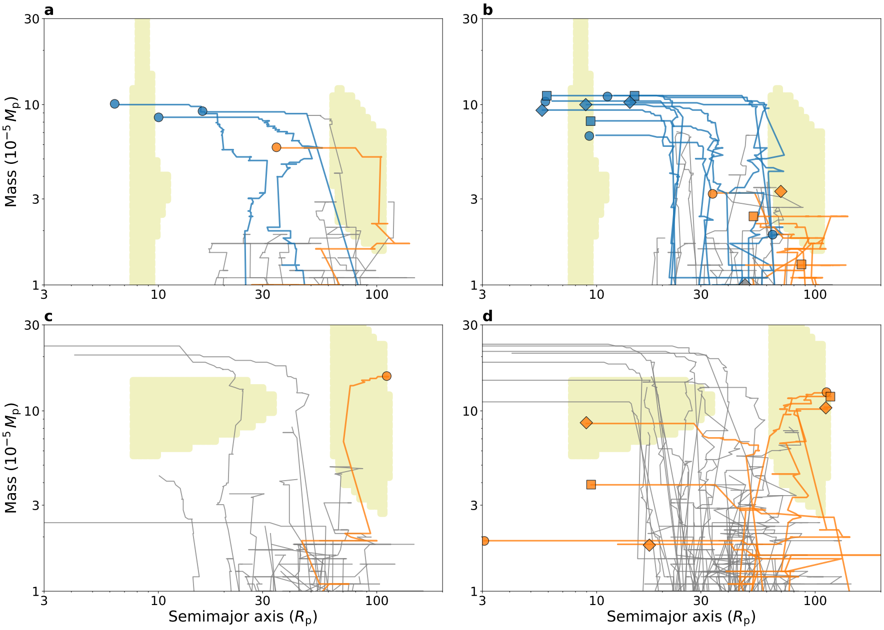

Supplementary Figure 6 Results of N-body simulations during the steady phase, where filled symbols represent satellites with the final mass greater than 10^{-5} $M_{\rm p}$. The colors indicate whether the satellites are in mean-motion resonance with their neighboring satellites: blue and orange circles denote those in and out of resonance. Resonance is defined as an orbital period ratio that deviates by no more than 2% from the exact integer ratio. The olive shaded area in the background represents the approximate safety zone where the orbital migration of the satellites could stop or even be directed outward. This region depends on the orbital eccentricity and inclination of the satellites, but in this figure, the eccentricity and inclination are assumed to be 0.01. For Jupiter, satellites can experience positive torque at the inner edge of CPDs at 8–9 $R_{\rm p}$. (a) The case of Jupiter shown in Figure 4 in the main text. (b) Three simulations performed under the same conditions as (a), but with different initial protosatellite positions. Results from the same run are represented by the same symbol. (c) The case of Saturn shown in Figure 4 in the main text. Titan's current semimajor axis is 20 $R_{\rm p}$. (d) Three simulations performed under the same conditions as (c), but with different initial protosatellite positions.

Supplementary Figure 6 presents the results of N-body simulations during the steady phase. Depending on the local slope of the gas density and temperature profile of CPDs, the positive corotation torque exerted on the satellite can exceed the negative Lindblad torque. In such cases, only satellites in specific regions (i.e., "the safety zone" shown in the olive shaded area) can avoid rapid inward migration. In fact, it has been shown that satellites migrate outward in regions where the local radial gradient of the disk temperature is steep [6].

Supplementary Figure 6(a) corresponds to the simulation shown in Figure 4 (Jupiter) of the main text. In the final configuration, the three inner satellites are in a 2:1 mean-motion resonance, while the outer satellite is out of resonance. The fact that the slower growth in the outer region makes the detached outer satellite, corresponding to Callisto, leading to a delayed onset of orbital migration. And the entry into the safety zone inhibits inward migration of the outer satellite.

Supplementary Figure 6(b) shows the results of three additional simulations performed under the same conditions as those in Supplementary Figure 6(a), but with different initial positions of protosatellites. The results observed in Supplementary Figure 6(a) are generally replicated in these simulations. Specifically, resonant satellites (blue) form in the inner orbits, while satellites detached from resonance (orange) form in the outer orbits. These satellites grow in the outer regions and migrate outward within the safety zone. Note that these results are from simulations of the steady phase. In the subsequent disk-dissipating phase, which evolves on a timescale of $\sim 100\,\mathrm{kyr}$, satellites generally undergo inward migration (see Figure 4).

Next, we examine the simulations of the Saturn system. Supplementary Figure 6(c) corresponds to the simulation results shown in Figure 4 (Saturn). Unlike in the case of Jupiter, there is no inner cavity in the CPD. Satellites that initiate inward migration fall into Saturn (gray). On the other hand, it can be observed that satellites growing in the outer region enter the safety zone and migrate outward. This eventually results in the survival of a single satellite, corresponding to Titan. Supplementary Figure 6(d) shows the results of three additional N-body simulations performed under the same conditions as those in Supplementary Figure 6(c). While many satellites fall into Saturn, the surviving satellites tend to grow in the outer region at $\simeq 100\,R_\mathrm{p}$ and are often susceptible to the safety zone. During this phase, the system may temporarily contain additional satellites on inner orbits ($\simeq 10\,R_\mathrm{p}$); however, over the $\sim 100\,\mathrm{kyr}$ duration of the disk-dissipating phase, a potential Titan located at $\simeq 100\,R_\mathrm{p}$ migrates inward, while satellites remaining on the inner orbits can be lost to Saturn in agreement with the ring formation model of [7].

In the N-body simulations discussed so far, the initial satellite mass of $10^{-6}\,M_\mathrm{p}$ was assumed. Supplementary Figure 7 shows how the initial satellite mass affects the results of satellite formation around Jupiter and Saturn, where the initial satellite mass is halved/doubled and the number of satellites is doubled/halved, with each case represented by three runs. In the case of Jupiter (Supplementary Figure 7(a) and (b)), similar results are obtained, with satellites in mean-motion resonances in the inner orbits and detached satellites in the outer orbits. In the case of Saturn (Supplementary Figure 7(c) and (d)), the results depend to some extent on the computational resolution. In the low-resolution case, only one out of 20 runs resulted in a satellite entering the outer safety zone around $100\,R_\mathrm{p}$, indicating that the formation of a potential

Titan is unlikely. In contrast, in the high-resolution case, while many satellites fall into Saturn (gray), some survive by entering the safety zone and avoiding inward migration. This outcome is consistent with the fiducial case.

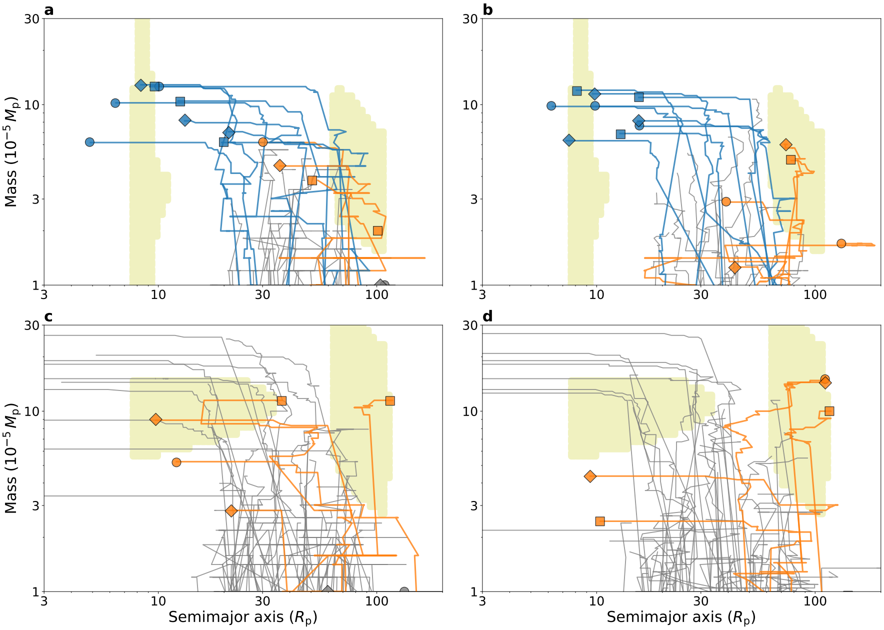

Supplementary Figure 7 Same as Supplementary Figure 6, but for different initial masses of protosatellites. (a) Low resolution simulation with initial mass of for $2 \times 10^{-6}\, M_{\mathrm{p}}$ Jupiter. (b) High resolution simulation with initial mass of $5 \times 10^{-7}\, M_{\mathrm{p}}$ for Jupiter. (c) Low resolution simulation with initial mass of $2 \times 10^{-6}\, M_{\mathrm{p}}$ for Saturn. (d) High resolution simulation with initial mass of $5 \times 10^{-7}\, M_{\mathrm{p}}$ for Saturn.

Finally, we comment on the statistics of the number of satellites formed in the N-body simulation results during the steady phase. In what follows, we quote the probabilities inferred from $n_{\mathrm{run}} = 20$ runs together with the 1σ binomial uncertainty, $\sigma = \sqrt{p(1-p)/n_{\mathrm{run}}}$, where p is the probability. Table 1 shows the percentages of runs classified by the number of satellites that remain in mean-motion resonance in the case of Jupiter and the presence or absence of additional satellites in non-resonant orbits, potential Callisto, outside these resonant satellites. In the fiducial models with the same conditions as those of the simulation shown in Figure 4, satellites in resonance form in 80%±9% of the cases in the presence of the inner cavity in the CPD. In addition, in 60%±11% of all simulations, an additional satellite is present in a non-resonant orbit outside the resonant satellites. Similar results were obtained in simulations with different resolutions. Table 1 also includes the case in which the initial satellite mass is reduced by half (i.e., the number of satellites is doubled) from the high-resolution setup. The probability of forming multiple satellites in resonance is 90%±7%, 80%±9%, 60%±11%, and 80%±9% for the low-, fiducial-, high-, and super-high resolution cases, respectively. The corresponding probabilities of forming a system with inner resonant satellites and an outer non-resonant Titan-like satellite are 55%±11%, 60%±11%, 40%±11%, and 60%±11%. Furthermore, the probability of forming systems most similar to the Jovian system with three inner resonant satellites and outer potential Callisto is 25%±10%, 40%±11%, 20%±9%, and 20%±9%, respectively. These probabilities are consistent within $\lesssim 2\sigma$ across different resolutions, indicating that the apparent non-monotonicity is dominated by stochasticity rather than a systematic resolution trend.

Table 1 Outcome fractions of satellites in resonance for Jovian systems (20 runs per set)

Set	Fraction of runs by number of satellites in resonance				Potential
	0	2	3	≥ 4	Callisto
Low resolution	0%	**25%**	**25%**	**5%**	Yes
	10%	10%	5%	20%	No
Fiducial	0%	**15%**	**40%**	**5%**	Yes
	20%	10%	10%	0%	No
High resolution	0%	**10%**	**20%**	**10%**	Yes
	40%	10%	5%	5%	No
Super high	0%	**30%**	**20%**	**10%**	Yes
	20%	0%	15%	5%	No

Note: Classification of the system by the number of large satellites with masses greater than $2 \times 10^{-5}\, M_{\mathrm{p}}$ that remain in mean motion resonances. The last column indicates whether any large satellites, potential Callisto, exist outside the inner resonance chain. Entries are percentages from $n_{\mathrm{run}} = 20$ runs in each case. Cases better matching the Jovian system are highlighted in bold.

Table 2 shows the percentages of runs classified by the number of satellites, excluding the potential Titan, remaining at the end of the steady-state phase in simulations of the Saturn system. In contrast to Jupiter, the number of remaining satellites is generally smaller. A potential Titan forms in the outer region with a probability of 35%±11% in simulations with the same conditions as those shown in Figure 4. The probability remains the same (35%±11%) even for cases that closely resemble the Saturn system, namely those in which a potential Titan is present and only 0–1 large satellites remain in the inner region. Examining the results at different resolutions, the formation probability of a potential Titan is 5%±5%, 35%±11%, and 50%±11% for the low-, fiducial-, and high-resolution cases, respectively, indicating that the probability is much lower in the low-resolution case. This is because satellites are less likely to enter the safety zone at 70–100 R_{p} in the low-resolution case. Therefore, low-resolution simulations may not be sufficient to resolve Titan formation. The probabilities of forming systems with a potential Titan and 0–1 inner large satellites are 5%±5%, 35%±11%, and 30%±10% for the low-, fiducial-, and high-resolution cases, respectively, showing no clear difference between the latter two. Note that this table reports the outcomes at the end of the steady-state phase. As shown in Figure 4 in the main text, in the Saturnian case, the satellites undergo substantial migration during the disk dissipating phase. We therefore expect that an inner satellite located at $\sim 10\,R_\mathrm{p}$ at the end of the steady phase will subsequently fall onto Saturn, and thus we also count cases with one remaining inner satellite as successful.

Table 2 Outcome fractions of satellites for Saturnian systems (20 runs per set)

Set	Fraction of runs by number of satellites excluding potential Titan				Potential
	0	1	2	3	Titan
Low resolution	**0%**	**5%**	0%	0%	Yes
	5%	60%	15%	15%	No
Fiducial	**10%**	**25%**	0%	0%	Yes
	10%	20%	30%	5%	No
High resolution	**5%**	**25%**	15%	5%	Yes
	5%	10%	35%	0%	No

Note: Classification of the system by the number of large satellites with masses larger than $2 \times 10^{-5}\,M_\mathrm{p}$ and semimajor axes larger than $3\,R_\mathrm{p}$, excluding potential Titan in the outer orbit. The last column indicates the presence of a potential Titan located beyond $100\,R_\mathrm{p}$, which migrates into the inner region during the disk dispersal phase. Results are summarized for 20 runs in each case. Cases better matching the Saturnian system are highlighted in bold.

To summarize the results of the N-body simulations at the end of the steady-state phase:

- In the case of the Jupiter system, the probability of forming a resonant chain in the inner region along with a potential Callisto in the outer region is 40–60%. In particular, several simulations (20–40%) result in the formation of three satellites in resonant orbits in the inner region and one detached satellite in the outer region.
- In the case of the Saturn system, about 30% of the simulations (in the fiducial and high-resolution cases) result in the formation of 0–1 inner satellites accompanied by a potential Titan in the outer region.
- The survival of Callisto and Titan can be explained by the inhibition of inward migration within the outer safety zone during the steady infall phase. Their current semimajor axes at $\simeq 20$ to $26\,R_\mathrm{p}$ can then be achieved during a 10 kyr period of inward migration as the infall rapidly ends (Figure 2(d)).

References

[1] French, M., et al., Ab Initio Simulations for Material Properties along the Jupiter Adiabat. Astrophys. J. Suppl. Ser. **202**(1), 5 (2012). https://doi.org/10.1088/0067-0049/202/1/5

[2] Murray, C.D., Dermott, S.F., Solar System Dynamics, (1999) https://doi.org/doi.org/10.1017/CBO9781139174817

[3] Lainey, V., Arlot, J.-E., Karatekin, Ö., van Hoolst, T., Strong tidal dissipation in Io and Jupiter from astrometric observations. Nature **459**(7249), 957–959 (2009). https://doi.org/10.1038/nature08108

[4] Lainey, V., et al., Resonance locking in giant planets indicated by the rapid orbital expansion of Titan. Nat. Astron. **4**, 1053–1058 (2020) arXiv:2006.06854. https://doi.org/10.1038/s41550-020-1120-5

[5] Bell, K.R., Lin, D.N.C., Using FU Orionis outbursts to constrain self-regulated protostellar disk models. Astrophys. J. **427**, 987–1004 (1994) astro-ph/9312015. https://doi.org/10.1086/174206

[6] Fujii, Y.I., Ogihara, M., Formation of single-moon systems around gas giants. Astron. Astrophys. **635**, 4 (2020) arXiv:2003.05052. https://doi.org/10.1051/0004-6361/201937192

[7] Canup, R.M., Origin of Saturn's rings and inner moons by mass removal from a lost Titan-sized satellite. Nature **468**(7326), 943–946 (2010). https://doi.org/10.1038/nature09661